



Title	Rh promoted In ₂ O ₃ as a highly active catalyst for CO ₂ hydrogenation to methanol
Author(s)	Dostagir, Nazmul Hasan M. D.; Thompson, Coogan; Kobayashi, Hirokazu; Karim, Ayman M.; Fukuoka, Atsushi; Shrotri, Abhijit
Citation	Catalysis science and technology, 10(24), 8196-8202 https://doi.org/10.1039/d0cy01789b
Issue Date	2020-12-21
Doc URL	http://hdl.handle.net/2115/83636
Type	article (author version)
Additional Information	There are other files related to this item in HUSCAP. Check the above URL.
File Information	SI_Rh_In ₂ O ₃ _1009.pdf (Supplementary information)



[Instructions for use](#)

Rh Promoted In₂O₃ as Highly Active Catalyst for CO₂ Hydrogenation to Methanol

Nazmul Hasan MD Dostagir,^{a,b} Coogan Thompson,^c Hirokazu Kobayashi,^a Ayman M.

Karim,^c Atsushi Fukuoka,^{*a} Abhijit Shrotri^{*a}

^aInstitute for Catalysis, Hokkaido University, Kita 21 Nishi 10, Kita-ku, Sapporo, Hokkaido 001-0021, Japan, email: ashrotri@cat.hokudai.ac.jp, fukuoka@cat.hokudai.ac.jp

^bGraduate School of Chemical Sciences and Engineering, Hokkaido University, Kita 13 Nishi 8, Kita-ku, Sapporo, Hokkaido 060-8628, Japan

^cDepartment of Chemical Engineering, Virginia Polytechnic Institute and State University, Blacksburg, Virginia 24060, United States

Table of contents

Materials and methods	2-6
Figure S1-S13	7-14
Table S1-S2	15-17
Results of DFT calculations with Figure S14, S15, and table S3-S7	18-25
References	26

Materials. Indium nitrate ($\text{In}(\text{NO}_3)_3 \cdot 3\text{H}_2\text{O}$), rhodium nitrate (aqueous solution of $\text{Rh}(\text{NO}_3)_3$ (25 wt.%) and nitric acid (9 wt.%), iron nitrate ($\text{Fe}(\text{NO}_3)_3 \cdot 9\text{H}_2\text{O}$), nickel nitrate ($\text{Ni}(\text{NO}_3)_2 \cdot 6\text{H}_2\text{O}$), cobalt nitrate ($\text{Co}(\text{NO}_3)_2 \cdot 6\text{H}_2\text{O}$), ruthenium chloride ($\text{RuCl}_3 \cdot x\text{H}_2\text{O}$), hydrogen hexachloroplatinate ($\text{H}_2\text{PtCl}_6 \cdot 2\text{H}_2\text{O}$), zinc nitrate ($\text{Zn}(\text{NO}_3)_2 \cdot 6\text{H}_2\text{O}$), citric acid, sodium carbonate (Na_2CO_3) and silicon carbide (SiC) (β form, particle size 50 nm) were purchased from Fujifilm Wako Pure Chemical Corporation. Palladium nitrate ($\text{Pd}(\text{NO}_3)_2 \cdot 2\text{H}_2\text{O}$) was bought from Sigma Aldrich.

Catalyst synthesis by co-precipitation and impregnation. For catalyst synthesis using co-precipitation method, 0.1 g/mL Na_2CO_3 solution was added dropwise to a 30 mL solution of $\text{In}(\text{NO}_3)_3 \cdot 3\text{H}_2\text{O}$ (4.75 mmol) and $\text{Rh}(\text{NO}_3)_3$ (0.062 mmol) under vigorous stirring until the pH became 9. After aging for 1h under stirring condition, the precipitate was centrifuged and washed thoroughly with water. It was dried at 130 °C in an oven for 12 h followed by calcination. The catalyst was named as Rh-1.3- In_2O_3 CP.

For catalyst prepared using wet impregnation, an equivalent amount of Rh present on the surface of Rh-1.3- In_2O_3 was loaded on In_2O_3 . In a typical procedure, In_2O_3 (0.5 g, prepared by sol-gel method) was dispersed in 30 mL of water followed by the addition of $\text{Rh}(\text{NO}_3)_3$ (20 μL of 0.0491 g mL^{-1} aqueous solution) and the mixture was kept under stirring at room temperature for 30 minutes. Water was evaporated under reduced pressure and then the powder was dried at 130 °C for 12 h followed by calcination. This catalyst was named as Rh/ In_2O_3 WI.

Catalyst Characterization. X-ray diffraction (XRD) was measured with Rigaku MiniFlex using $\text{CuK}\alpha$ X-ray ($\lambda = 1.54 \text{ \AA}$) operating at 40 kV and 20 mA. N_2 adsorption isotherms were

measured at $-196\text{ }^{\circ}\text{C}$ using a Belsorp mini analyzer. Prior to the adsorption, all samples were degassed under vacuum at $120\text{ }^{\circ}\text{C}$ for 2 h. Surface area was calculated by using BET theory between the relative pressure range 0.05 to 0.35 in the N_2 adsorption isotherm.¹ X-ray photoelectron spectroscopy (XPS) was performed with JEOL JPS-9010MC instrument. Charge correction was made by adjusting the external carbon peak to 284.6 eV. STEM image was obtained in a JEOL JEM-ARM200F atomic resolution electron microscope at an acceleration voltage of 200 kV equipped with EDS detector EX-24221M1G5T.

Data processing for X-ray absorption fine structure (XAFS) analysis. Data processing and analysis, for the x-ray absorption near edge and the extended x-ray absorption fine structure (XANES and EXAFS), were performed using Athena and Artemis programs of the Demter data analysis package.² After the normalization of the absorption coefficient, the smooth atomic background was subtracted using the AUTOBKG code in Athena to obtain $\chi(k)$ (where k is the photoelectron wave number). The theoretical EXAFS signal for Rh-O, and Rh-In scattering paths were constructed using the FEFF6³ code using the crystal structure of In_2O_3 and replacing the central In atom with a Rh atom.³ The theoretical EXAFS signals were fitted to the data in r -space using Artemis. The spectra were fitted by varying the coordination number of the single scattering paths, Rh-O and Rh-In/Rh, the effective scattering lengths, the bond length disorder of each path and the correction to the threshold energy, ΔE_0 (ΔE_0 was the same since all the paths were calculated using the same model). S_0^2 (the passive electron reduction factor) was obtained by first analyzing the spectrum for a Rh foil, and the best fit value (0.85) was fixed during the fitting. The k -range used for Fourier Transform of the $\chi(k)$ was $3\text{-}13.9\text{ \AA}^{-1}$ and the r -range for fitting was $1.2\text{-}2.0\text{ \AA}$ for fitting Rh-O scattering path only and $1.2\text{-}4.0\text{ \AA}$ for fitting the

full model including Rh-O and Rh-Rh paths. The best parameters fit using a k-weight of 1,2,3 (simultaneously) in Artemis are reported, however, the results were similar to those using only a k-weight of 2.

Equations. CO₂ conversion, selectivity of CO and CH₃OH and space time yield (STY) of CH₃OH were calculated using the following equations.

CO₂ conversion:

$$X_{(CO_2)} = \left(\frac{nCO_{out} + nCH_3OH_{out}}{nCO_{2\ out} + nCO_{out} + nCH_3OH_{out}} \right) \times 100\%$$

CO and CH₃OH selectivity

$$S_{(CO)} = \left(\frac{nCO_{out}}{nCO_{out} + nCH_3OH_{out}} \right) \times 100\%$$

$$S_{(CH_3OH)} = \left(\frac{nCH_3OH_{out}}{nCO_{out} + nCH_3OH_{out}} \right) \times 100\%$$

Space time yield (STY) of methanol:

$$STY_{(CH_3OH)} = \left(\frac{SV \times [CO_2] \times X_{(CO_2)} \times S_{(CH_3OH)} \times M_{(CH_3OH)}}{22400} \right)$$

Where nCO_{2 out}, nCO_{out}, nCH₃OH_{out} are moles of CO₂, CO and CH₃OH calculated from GC analysis. SV is space velocity in mL h⁻¹ g⁻¹, [CO₂] is the concentration of CO₂ present in the feed gas mixture in %, and M_(CH₃OH) is molecular weight of methanol in g mol⁻¹. STY of CH₃OH is reported in g_{MeOH} h⁻¹ g_{cat}⁻¹.

DFT calculations. We used the Gaussian 16 rev. A.03 program and initially built a $\text{In}_{24}\text{O}_{36}$ cluster to qualitatively evaluate the chemical reactions on In_2O_3 (110) surface, where the initial geometry was the same as that of crystal In_2O_3 . The DFT calculations for Rh doping on the surface were performed by using the PBE functional with the density fitting approximation.⁴ Basis sets were def2-SVP for the central three metal atom sites that were potential Rh doping sites; 6-31+G(d) for O atoms surrounding the three metal atoms; 3-21+G for other O atoms; LanL2DZ for In atoms in vicinal positioning to O atoms with the 6-31+G(d) basis set; LanL2MB for other In atoms (see Fig. S14).⁵ This combination was used to decrease the number of basis as much as possible so that the self-consistent field calculations converged within acceptable time (*ca.* one week using an Intel Xeon Gold 6142 processor). Suitable effective core potential (ECP) was applied for Rh and In atoms. Empirical dispersion was included by Grimme's D3 function.⁶ Spin multiplicity was optimized, and the self-consistent field solution was re-optimized with the *stable=opt* option to find the most stable electronic state in all calculations. The material had three possible sites for Rh (M_1 to M_3 in Fig. S14), locating at the center of the model. After replacing one In atom with Rh, orientation of the three metal sites and surrounding O atoms was optimized, where other atoms were frozen to preserve the crystal structure. We used the *loose* level of geometry optimization [root mean square (RMS) force < 0.001667 a.u., RMS displacement < 0.006667 a.u.] to decrease calculation time. Error in electronic energy due to use of the *loose* option was less than 0.1 kJ mol^{-1} , which was accurate enough to discuss the Rh sites.

Other calculations were performed after reducing the number of atoms to 40 (Fig. S15a) at the PBE0-D3 level of theory with the *tight* level of geometry optimization (RMS force < 0.00045

a.u., RMS displacement < 0.0012 a.u.), and zero-point vibration energy was involved in the energy calculations.⁷ Basis sets were slightly improved (Fig. S15a), compared to that employed for the 60-nuclei system. The In atom at the central light blue atom, corresponding to M₃ in Fig S14, was replaced with Rh when effect of doping was evaluated. To calculate the removal energy of lattice oxygen, oxygen atoms surrounding M₃ (In or Rh) were removed by the following equation: $\text{MO}_x + \text{H}_2 \rightarrow \text{MO}_{x-1} + \text{V}_\text{O} + \text{H}_2\text{O}$. For the evaluation of CO₂ activation, CO₂ was located above the left (M₂) and the central light blue metal (M₃) atoms after removing a designated number of lattice oxygen atoms around M₃. In the transition state calculations, we found only one imaginary frequency vibration and intrinsic reaction coordinates (IRC) that connect expected substrates and products.

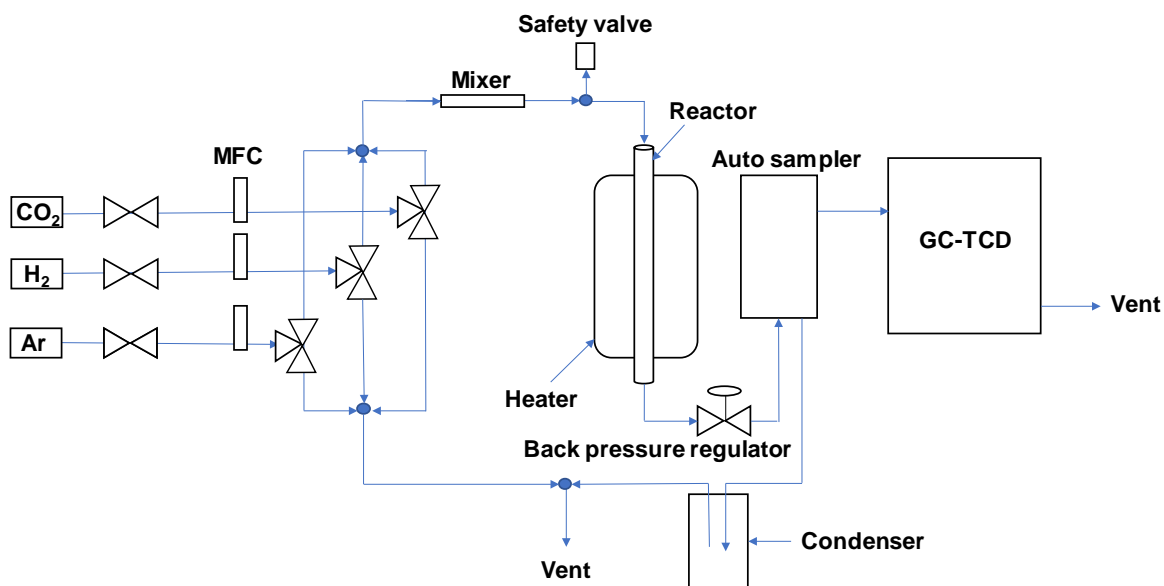


Fig. S1. Schematic representation of reaction set up.

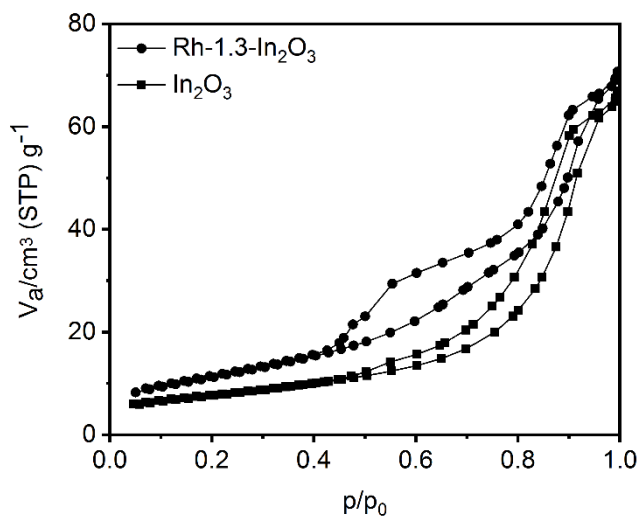


Fig. S2. N_2 adsorption isotherm of In_2O_3 and $\text{Rh-1.3-In}_2\text{O}_3$.

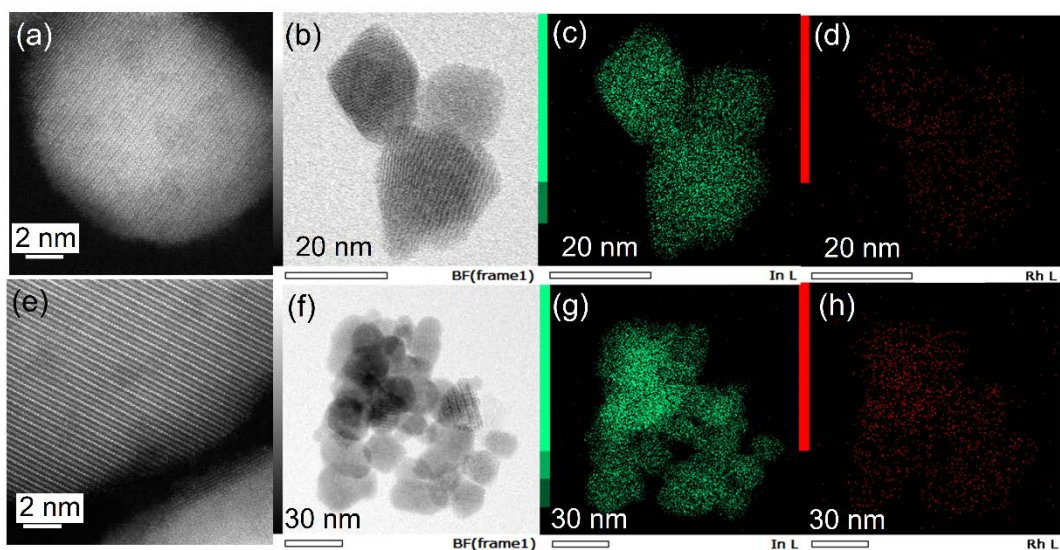


Fig. S3. HAADF-STEM images for fresh (a) and used (e) Rh-1.3-In₂O₃ catalysts. EDX mapping for fresh (b,c,d) and used (f,g,h) catalysts.

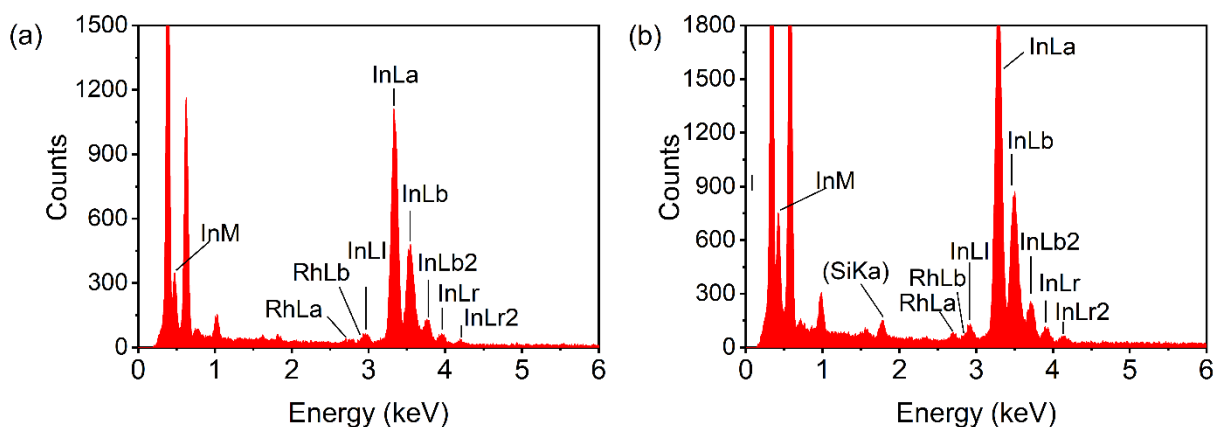


Fig S4. Corresponding EDX spectra of (a) fresh and (b) used Rh-1.3-In₂O₃ catalysts showing EDX signature peaks for Rh and In. SiKa was detected in used catalyst because of the presence of quartz wool used during the reaction.

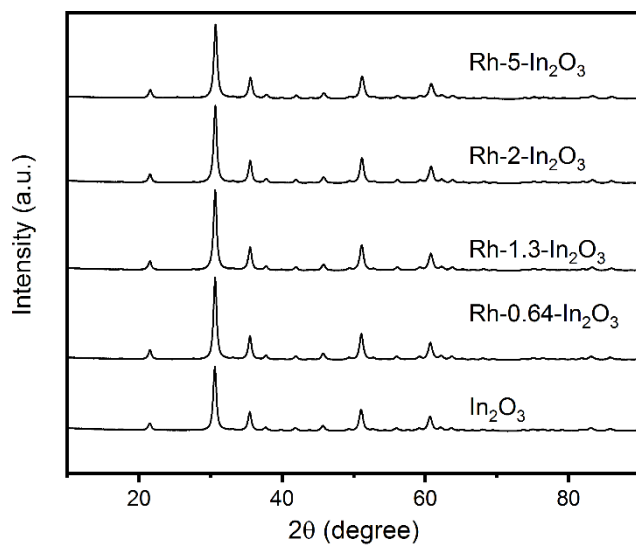


Fig. S5. XRD patterns of all catalysts. Only peaks for cubic In₂O₃ were observed at all Rh loadings.

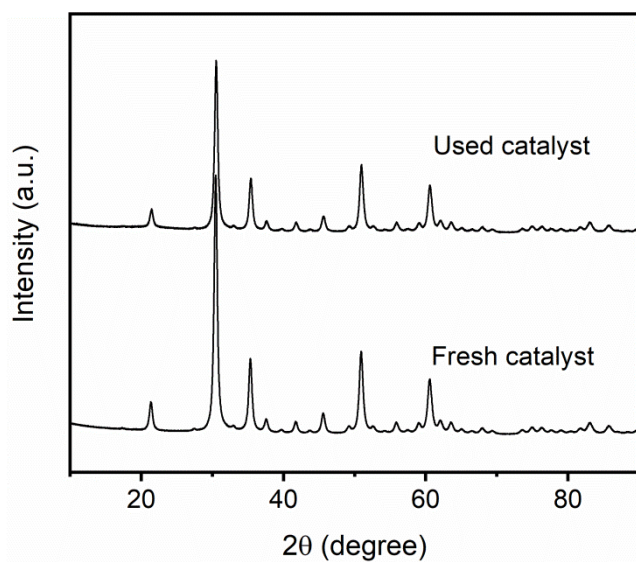


Fig. S6. XRD of fresh and used Rh-1.3-In₂O₃ catalysts.

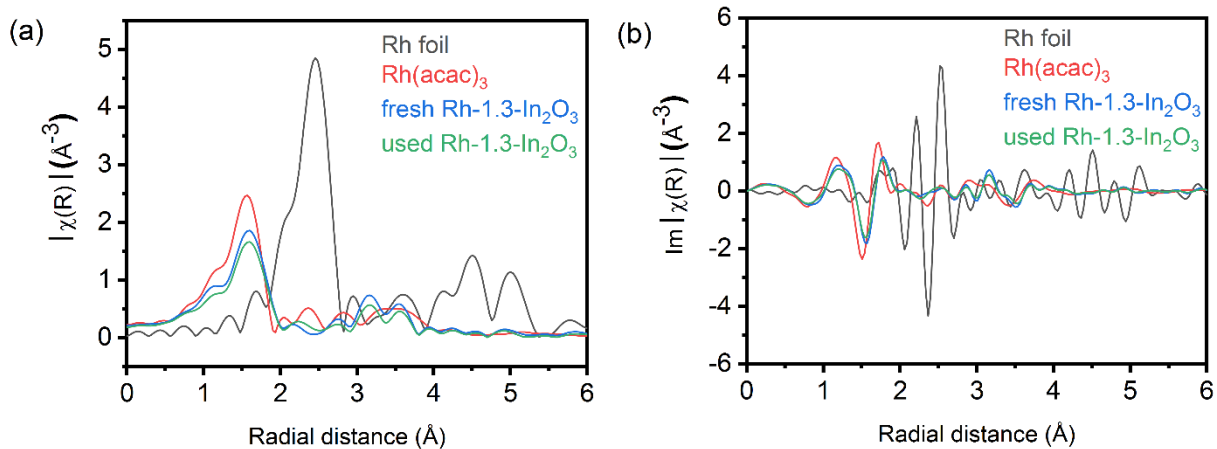


Fig. S7. (a) Magnitude and (b) imaginary part of the Fourier transformed k^2 -weighted $\chi(k)$ data ($\Delta k = 3-13 \text{ \AA}^{-1}$) in R space for both the fresh and used Rh-1.3-In₂O₃ catalysts along with Rh(acac)₃ and Rh foil as references.

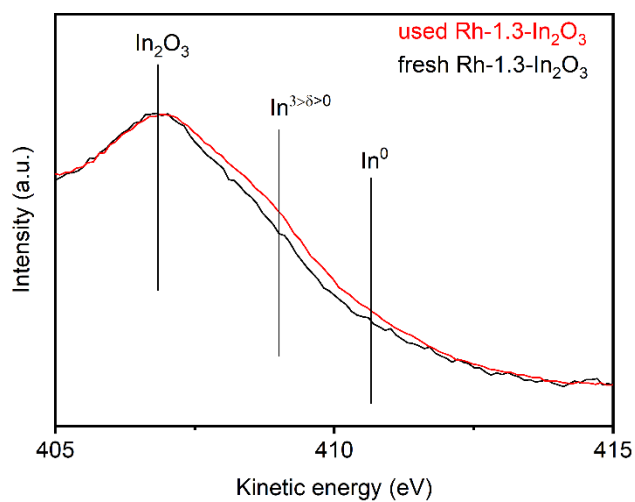


Fig. S8. In MNN peak of fresh and used Rh-1.3-In₂O₃ catalysts.

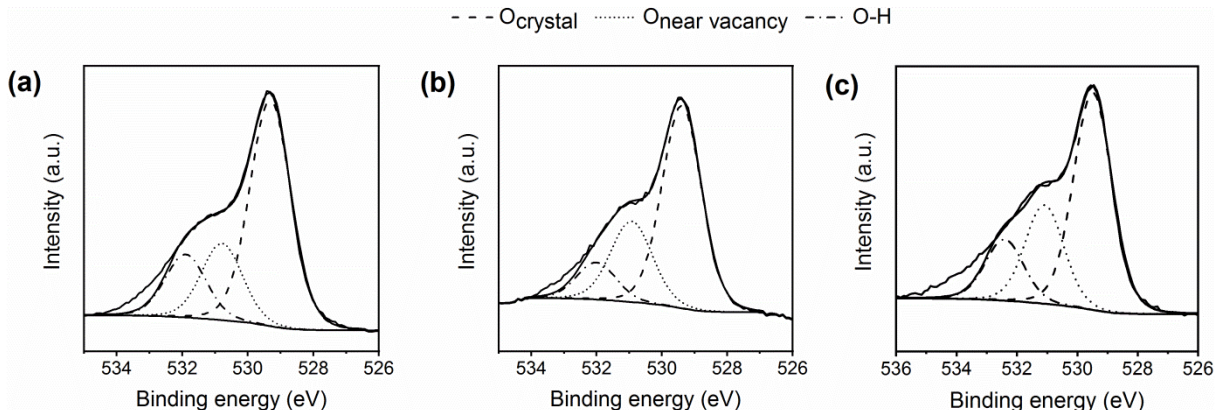


Fig. S9. O 1s XPS spectra of (a) In_2O_3 , (b) fresh Rh-1.3- In_2O_3 and (c) used Rh-1.3- In_2O_3 .

In_2O_3 has oxygen vacancies within its crystal structure, which gives rise to a peak at 530.9 eV in XPS corresponding to oxygen atoms adjacent to the vacancy ($\text{O}_{\text{near vacancy}}$). The oxygen in surface hydroxyl groups appeared as a peak at 532 eV. The cumulative of these two oxygen species is referred as defective oxygen.

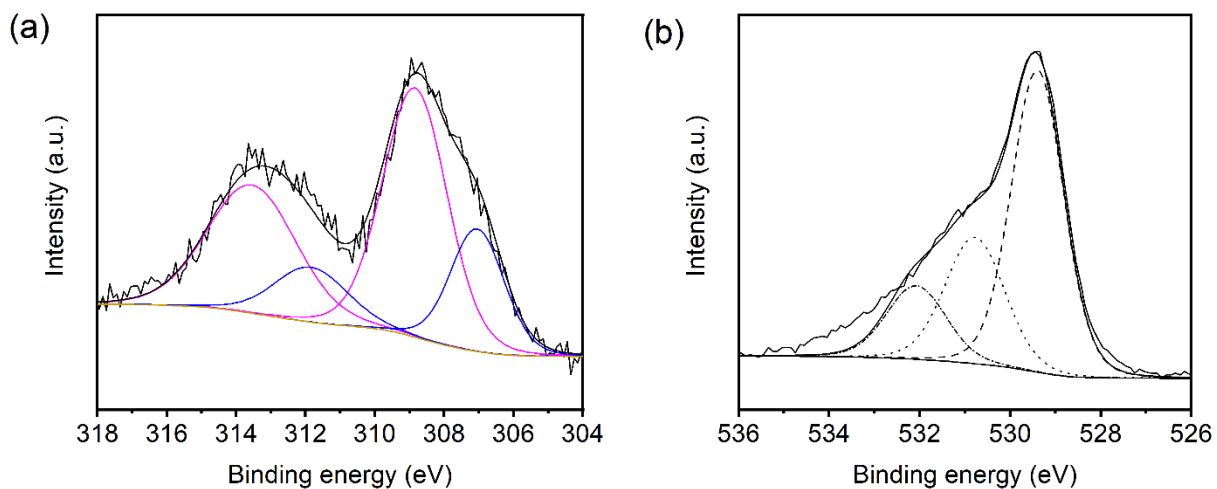


Fig. S10. XPS analysis of (a) Rh 3d and (b) O 1s after reaction for 1h. Purple and blue lines show fitting of Rh^{3+} and reduced Rh species respectively.

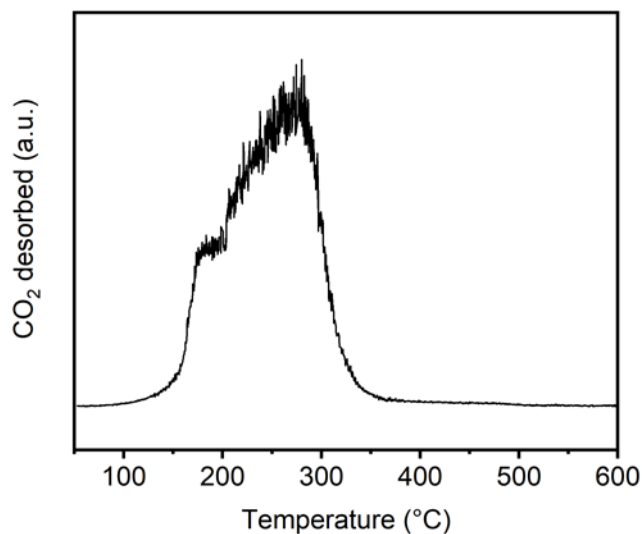


Fig. S11. Mass spectrum for evolution of CO₂ during TPD of formic acid impregnated Rh-1.3-In₂O₃ catalyst.

Figure S11 shows the evolution of CO₂ gas due to decomposition of adsorbed formic acid on the catalysts surface. The peak at 270 °C appeared at the same temperature (main manuscript, Figure 6, red line) compared to CO₂ TPD after exposing the catalyst to condition similar to reaction condition, suggesting the formation of formates species during CO₂ hydrogenation.

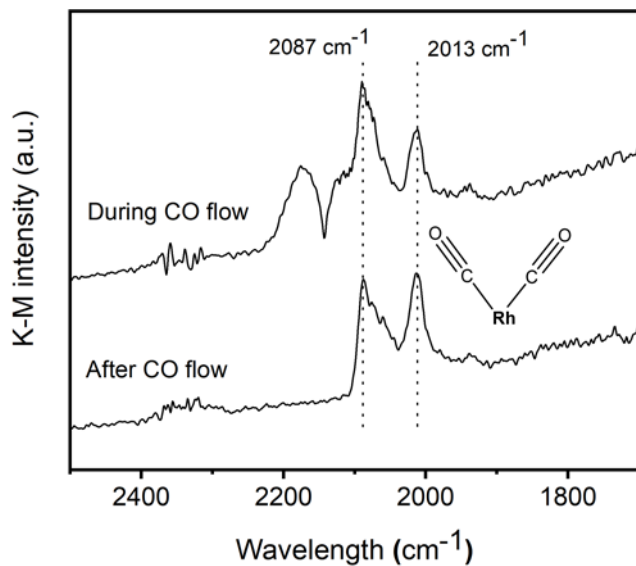


Fig. S12. CO DRIFTS over Rh-1.3-ZnO.

Adsorption of CO over Rh-1.3-ZnO catalyst shows peaks at 2087 and 2013 cm⁻¹ in figure S12 which were attributed to the vibration (symmetric and asymmetric) of CO on single Rh atom, *gem*-dicarbonyl Rh(CO)₂. This suggests the atomic Rh dispersion in Rh-1.3-ZnO.⁸

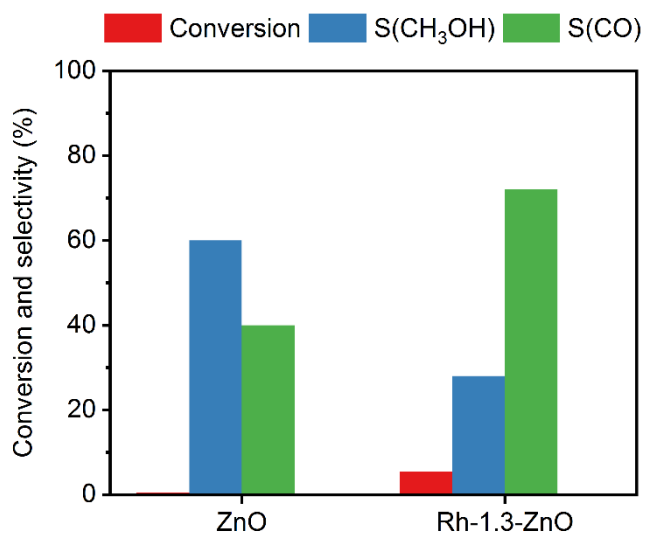


Fig. S13. Comparison of catalytic activity for CO₂ hydrogenation between ZnO and Rh-1.3-ZnO (reaction condition: 300 °C, 5 MPa, 60,000 mL h⁻¹ g_{cat}⁻¹, H₂/CO₂ = 4).

Table S1. XRD analysis of In₂O₃ and Rh-X-In₂O₃ catalysts.

Rh mol %	2 θ (degree)	d spacing (Å)	Lattice parameter (a) (Å)
0	30.57	2.921	10.1186
0.64	30.60	2.918	10.1082
1.3	30.61	2.917	10.1048
2	30.63	2.915	10.0978
5	30.66	2.912	10.0875

Table S2. Results of fitting of the EXAFS spectra for fresh and used Rh-1.3-In₂O₃ catalysts and Rh(acac)₃ used as reference.

Sample	Fresh ^a	After reaction ^a	Rh(acac) ₃
$N_{\text{Rh-O}}$	6.1±0.7	5.2±0.6	6.4±0.9
$R_{\text{Rh-O}} (\text{Å})$	2.05±0.01	2.05±0.01	1.99±0.01
$\sigma^2_{\text{Rh-O}} \times 10^3 (\text{Å}^2)$	5±1	4±1	2±2
$\Delta E_{\text{0 Rh-O}} (\text{eV})$	7.0±1.3	8.3±1.2	7.9±1.9
$N_{\text{Rh-In/Rh}}$	5.3±1.8	5.3±1.8	-
$R_{\text{Rh-In/Rh}} (\text{Å})$	3.30±0.01	3.30±0.02	-
$\sigma^2_{\text{Rh-In/Rh}} \times 10^3 (\text{Å}^2)$	8±2	9±3	-
$\Delta E_{\text{0 Rh-In/Rh}} (\text{eV})$	7.0±1.3	8.3±1.2	-
$N_{\text{Rh-In/Rh}}$	4.5±2.7	3.0±2.5	-
$R_{\text{Rh-In/Rh}} (\text{Å})$	3.82±0.03	3.83±0.03	-
$\sigma^2_{\text{Rh-In/Rh}} \times 10^3 (\text{Å}^2)$	8±4	7±5	-
$\Delta E_{\text{0 Rh-In/Rh}} (\text{eV})$	7.0±1.3	8.3±1.2	-
Reduced χ^2	249	199	9433
R-factor	0.0086	0.0094	0.0022

^aThe coordination numbers and bond lengths for the Rh-O path in both catalysts were almost identical for the models with and without the Rh-In scattering paths. Note that the scattering from In and Rh have similar phase shift due to their similar atomic numbers. Therefore, the scattering from labelled Rh-In can also be Rh-Rh, however, the low weight loading of Rh suggests that the scattering is from In and not from Rh.

Notation: N , coordination number of absorber-backscatterer pair; R , radial absorber-backscatterer distance; σ^2 , the mean square displacement of the half-path length and represents the stiffness of the bond for a single scattering path, ΔE_0 , correction to the threshold energy.

Results of DFT calculations.

An $\text{In}_{24}\text{O}_{36}$ cluster model with atomic arrangement similar to 110 plane of In_2O_3 , known to be the active plane for CO_2 reduction, was doped with Rh (Fig. S14). As this model contains influence of dangling bonds at the edge near reaction centers ($\text{M}_1\text{--M}_3$), the calculations are used for qualitative understanding of the molecular level behaviors of the material. The electronic energy evaluation suggested that Rh preferred the M_2 and M_3 sites, which were octahedral sites with five O coordination (RhO_5 ; Table S3). We decided to put Rh at the M_3 site as a representative promising site for Rh doping. In this case, the average Rh–O bond length (2.05 Å) in the model was found to be similar to that determined from EXAFS analysis of the catalyst, which suggested that this model is similar to the real Rh-doped In_2O_3 .

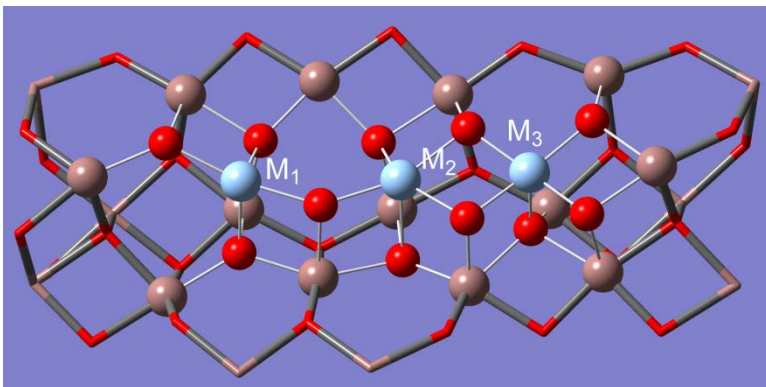


Fig. S14. $\text{In}_{24}\text{O}_{36}$ model employed in the DFT calculations for evaluating possible Rh sites. Basis sets: light blue metal atoms ($\text{M}_1\text{--M}_3$): def2-SVP; O atoms shown as red balls: 6-31+G(d); In atoms shown as brown balls: LanL2DZ; O atoms depicted as red stick: 3-21+G; In atoms depicted as brown stick: LanL2MB.

Table S3. DFT calculations for the Rh doping at the In sites on In_2O_3 (110) plane using a 60 nuclei model.^a

Rh site ^a	$\Delta E(\text{electronic}) / \text{kJ mol}^{-1}$
M_1	+33.2
M_2	+9.9
M_3	0

^aIn atoms at M_1 to M_3 sites (Fig. S14) were replaced with a Rh atom.

For the roles of Rh on the formation of oxygen vacancy, we prepared a 40-nuclei model (Fig. S15a), a partial structure of that in Fig. S14. The M_3 site was doped with Rh as discussed above. Hydrogenation condition removed four O atoms around the Rh in a thermodynamically favored manner (RhO , $\Delta E = -110 \text{ kJ mol}^{-1}$; Fig. S15b, red line), and the Rh atom was stabilized by the interaction with neighboring In atoms. In contrast, undoped In_2O_3 lost only one O atom around the In atom at the same site owing to large uphill nature of the second reduction (Fig. S15b, blue line), thus suggesting that Rh facilitates the formation of a higher density of oxygen vacancies, compared to In atoms.

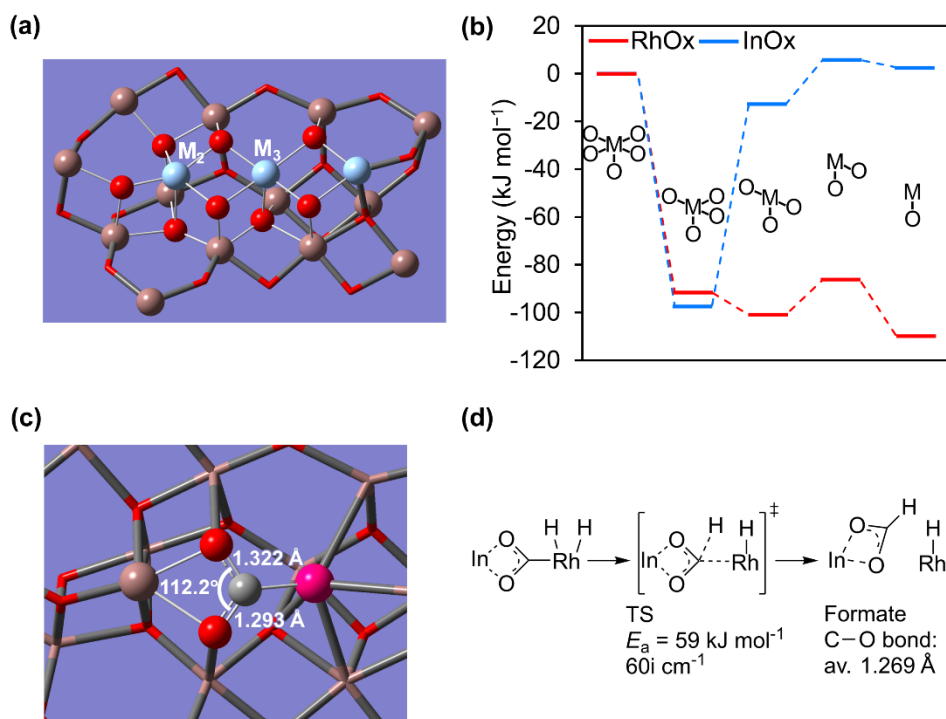


Fig. S15. Model for evaluating oxygen vacancy formation and CO_2 activation. (a) structure of this system, (b) the removal of lattice oxygen around surface Rh or In ($\text{MO}_x + \text{H}_2 \rightarrow \text{MO}_{x-1} + \text{V}_\text{O} + \text{H}_2\text{O}$), (c) CO_2 adsorption on RhO site and (d) reduction of the CO_2 , where only the important centers are depicted. Gray: C; pink purple: Rh. M_2 and M_3 are corresponding to the same sites in Fig. S14. Basis sets: light blue metal atoms: def2-SVP; O atoms shown as red balls: 6-31++G(d); In atoms shown as brown balls: LanL2DZ; O atoms depicted as red stick: 3-21+G. The 6-31++G(d) basis set was applied for additional atoms (CO_2 and H_2).

We also studied the activation of CO₂ and the hydrogenation to formate, the intermediate detected in the real experiments. Introduction of a CO₂ molecule onto the RhO site produced a Rh-COO species of which the O atoms occupied two oxygen vacant sites ($\Delta E = -159 \text{ kJ mol}^{-1}$; Fig. S15c). The C-O bond lengths were 0.13 and 0.16 Å longer than that of gaseous CO₂. Moreover, the COO moiety had a bending angle of 112° and a CM5 charge⁹ of -0.43e, thus showing activation of CO₂.¹⁰ Hydrogen addition to the activated CO₂ was tested after coordinating two H atoms on Rh. The H₂ dissociation to produce Rh(-H)₂ was energetically favorable (-54 kJ mol⁻¹). The H species smoothly attacked the activated CO₂ and successively Rh-C bond was cleaved to give formate with a low activation energy of 59 kJ mol⁻¹ (Fig. S15d). The transition state appeared in the step of Rh-C bond scission rather than H transfer, thereby having a low imaginary vibration frequency (60i cm⁻¹). We also calculated a one H system, namely hydrogenation of CO₂ not by Rh(-H)₂ but by Rh-H. In this case, the H transfer gave a transition state with a low activation energy of 46 kJ mol⁻¹. Thus, in both cases, formate was produced by activated H species on Rh. Contrastingly, introduction of CO₂ on undoped In₂O₃ produced non-activated carbonate species (not shown). Therefore, we propose that Rh can be involved in the activation of CO₂ and the hydrogenation.

The atomic coordinates for the important structures are available as follows: Rh doping at the M₃ site (Table S4); CO₂ adsorption on Rh-doped In oxide cluster (Table S5); transition state for CO₂ hydrogenation by Rh(-H)₂ (Table S6); transition state for CO₂ hydrogenation by Rh-H (Table S7).

Table S4. Atomic coordinate and basis sets for Rh-doped In oxide cluster in a format of Gaussian input.

0	7			
In	0	-3.42265400	-0.05667000	-1.50558300
In	0	0.63949200	0.00526900	-1.31349300
Rh	0	3.94448100	-0.00971700	-1.40172400
O	0	-5.29742900	-0.99376800	-1.97319600
O	0	-3.02971800	-1.74898200	-0.22435100
O	0	-3.63749700	1.11158900	0.30563100
O	0	-1.39698900	0.65734600	-1.41484900
O	0	-0.05041700	-1.74691100	0.18206000
O	0	0.49393700	1.27426200	0.82587400
O	0	2.38271100	-1.29314400	-1.43210300
O	0	2.36001100	1.27530000	-1.58216900
O	0	3.80076800	0.72026100	0.45742000
O	0	5.57930200	-1.25739400	-1.66858000
O	0	5.42826000	1.32980300	-1.65759800
In	-1	0.25780700	-0.62518800	1.87010200
In	-1	1.87926200	-2.84644600	-0.12729300
In	-1	-3.63580600	-0.69040000	1.64335200
In	-1	-1.63864800	1.82223600	0.46722400
In	-1	-5.53731000	2.02079000	0.79663900
In	-1	-1.50242700	-3.24891700	-0.41762500
In	-1	-7.31243000	-0.16706600	-1.92436900
In	-1	-4.90380600	-2.95028100	-0.58529200
In	-1	5.64156000	2.02525700	0.42765900
In	-1	4.15144800	-0.55967600	2.09632500
In	-1	2.24001300	2.32279600	0.25967400
In	-1	5.77750900	-3.04578900	-0.45652200
In	-1	7.24710700	0.23940000	-2.00227100
O	-1	-5.16802900	3.45647500	-0.78931200
O	-1	-7.46692900	3.19078300	0.87337700
O	-1	-1.80254300	3.62378100	-0.73355300
O	-1	4.10472400	3.55021700	0.60139400
O	-1	7.09332300	3.59678800	0.79521600
O	-1	1.77090700	4.14131700	-0.95063100
O	-1	2.26381700	-1.52581900	1.63134700
O	-1	-1.74795800	0.27545800	2.10830700
O	-1	0.40879900	-4.38889700	-0.79868500
O	-1	-8.70311500	-2.15747200	1.36260000
O	-1	-5.33302300	-2.15776100	1.38912800
O	-1	-8.71135300	0.50144000	2.42870900
O	-1	-8.94597800	-1.65066800	-1.57937900
O	-1	-6.67375400	-4.18691500	-0.35927600
O	-1	-7.00811300	0.47968600	0.12549200
O	-1	-5.34128700	0.50123600	2.45524700
O	-1	-3.34836700	-4.54873600	-0.46235500
O	-1	-9.08642600	1.20873200	-1.68256100
O	-1	5.85723700	-1.75150600	1.28434600
O	-1	9.22728800	-1.75169900	1.31089600
O	-1	5.84887700	0.90747400	2.35052800
O	-1	9.18772600	-0.72736000	-1.87503800
O	-1	7.88651500	-3.78087900	-0.43728400
O	-1	7.55264100	0.88543500	0.04735200
O	-1	3.70950900	-3.84019000	-0.74307700
In	-1	-3.55545700	4.96984200	-0.81300900
In	-1	9.02299300	2.42680000	0.71846300
In	-1	-8.91948800	1.61970200	0.50650600
In	-1	-7.02218800	-0.82812000	1.90891800
In	-1	7.53795800	-0.42214700	1.83078500
In	-1	9.65659200	-2.54455000	-0.66386400
In	-1	-8.78284800	-3.45177200	-0.37840300

In -1 -0.16890400 5.10744100 -1.07853200

Table S4 continue

1-3 0
def2SVP

4-14 0
6-31+G(d)

15-27 0
LanL2DZ

28-52 0
3-21+G

53-60 0
LanL2MB

1-3 0
def2SVP
15-27 0
LanL2DZ
53-60 0
LanL2MB

Table S5. Atomic coordinate and basis sets for CO₂ adsorption on Rh-doped In oxide cluster in a format of Gaussian input.

```

0 5
Rh      0    1.52811300  -0.22590400  -0.70777700
In      0   -2.83281100  -0.31314100  -1.05182100
In      0    3.98855800  -0.12681300  -1.87243200
O       0    0.44891200   1.03149600   0.70681300
O       0   -2.64596800   0.98081300   0.73594300
O       0   -2.88649800  -1.99236800   0.37909900
O       0   -4.75998300   0.16647200  -1.18440600
In     -1   -3.87587500   4.72743900  -1.08937700
In     -1   -2.70128500  -0.77391800   2.08867900
In     -1   -0.98538800  -2.92723200   0.09779700
In     -1   -4.91441000   1.40029800   0.69763000
In     -1   -4.32035100  -3.67257700   0.04290900
In     -1   -6.61576000  -0.79908600  -1.25740700
In     -1    2.29309300   2.30945700   0.18229100
In     -1    1.17269600  -0.31578400   2.06305700
In     -1    4.50668300   0.13712300   1.57573500
In     -1    5.62864200   3.05517200   0.23950500
In     -1   -1.12501200   2.26622500   0.22094800
In     -1    2.88717500  -2.76198400  -0.47048700
In     -1    6.67684400  -1.89713600  -0.94859700
O      -1   -5.32867100   3.11184900  -0.57196000
O      -1    0.62464800   3.68540200   0.38430600
O      -1    3.59927200   4.03334000   0.38465700
O      -1   -1.84456000   3.96339000  -1.04076200
O      -1   -0.63231300  -1.48521000   1.76542600
O      -1   -4.76991300  -0.06133700   2.41273400
O      -1   -2.32988000  -4.63930900  -0.40631600
O      -1   -6.90527700   0.39453300   0.58180000
O      -1   -5.98950700  -2.29869500   0.24271300
O      -1    2.93854100  -1.37737900   1.20010200
O      -1    6.28729400  -1.04690700   1.01096000
O      -1    2.72575300   1.32113400   2.13993700
O      -1    5.95725000  -0.19815700  -2.21002000
O      -1    5.05681600  -3.28618000  -0.55169000
O      -1    4.28425100   1.34192100  -0.26185800
O      -1    0.89624100  -3.76886500  -0.58746200
C       0   -0.19593200  -0.15444700  -1.53206300
O       0   -0.90295000  -1.27159500  -1.52923100
O       0   -0.94179800   0.89542900  -1.64586500

1-3 0
def2SVP
****
4-7 37-39 0
6-31+G(d)
****
8-20 0
LanL2DZ
****
21-36 0
3-21+G
****

1-3 0
def2SVP
8-20 0
LanL2DZ

```

Table S6. Atomic coordinate and basis sets for the transition state of CO₂ hydrogenation by Rh(-H)₂ in a format of Gaussian input.

```

0 3
Rh      0    1.57660500   -0.50034900   -1.31014100
In      0   -2.94023000   -0.34661100   -0.97061700
In      0    4.01642500   -0.00869900   -1.84671000
O       0    0.60245400    0.98793400    0.39215100
O       0   -2.61198000    0.99184200    0.75170800
O       0   -2.89112000   -1.98274100    0.42577400
O       0   -4.81417100    0.23658500   -1.17485000
In     -1   -3.86020900    4.73856000   -1.07858400
In     -1   -2.70109800   -0.74644300    2.13397000
In     -1   -0.98122700   -2.91235800    0.15972800
In     -1   -4.90712700    1.42302900    0.72329400
In     -1   -4.31700000   -3.65453200    0.09925800
In     -1   -6.60562600   -0.78599600   -1.22378300
In     -1    2.30235900    2.31993000    0.22491400
In     -1    1.17368600   -0.29190000    2.11653700
In     -1    4.50946900    0.15448700    1.63691400
In     -1    5.63836900    3.06398000    0.28758600
In     -1   -1.11507400    2.28094000    0.25424300
In     -1    2.89214600   -2.75295900   -0.39716100
In     -1    6.68504800   -1.89624100   -0.86938100
O      -1   -5.31634400    3.12741300   -0.55641600
O      -1    0.63458100    3.70047200    0.41396400
O      -1    3.60954300    4.04512600    0.42097300
O      -1   -1.82992500    3.97272800   -1.01957400
O      -1   -0.63169000   -1.46145300    1.82045200
O      -1   -4.76971300   -0.02963000    2.44742500
O      -1   -2.32625900   -4.62580400   -0.33865400
O      -1   -6.89911900    0.41820400    0.60788900
O      -1   -5.98520000   -2.27779400    0.28642800
O      -1    2.94122800   -1.36064800    1.26518300
O      -1    6.29057200   -1.03459000    1.08395800
O      -1    2.72826200    1.34354100    2.18927700
O      -1    5.97081400   -0.20356100   -2.14269700
O      -1    5.06224300   -3.28149700   -0.47041800
O      -1    4.29440200    1.34870500   -0.20758700
O      -1    0.90147700   -3.75992300   -0.51552700
C       0   -0.60165800   -0.24298800   -2.12570100
O       0   -1.15914800   -1.36162500   -1.80153100
O       0   -1.24001700    0.83155600   -1.92981100
H       0    0.38401000   -0.25200500   -2.71579300
H       0    2.08588500   -1.44728400   -2.41878900

```

```

1-3 0
def2SVP
****
4-7 37-41 0
6-31++G(d,p)
****
8-20 0
LanL2DZ
****
21-36 0
3-21+G
****

```

```

1-3 0
def2SVP
8-20 0
LanL2DZ

```

Table S7. Atomic coordinate and basis sets for the transition state of CO₂ hydrogenation by Rh-H in a format of Gaussian input.

```

0 4
Rh      0    1.51495000  -0.26201400  -0.97009300
In      0   -2.91139200  -0.34992400  -1.02019900
In      0    4.01327800  -0.11830600  -1.85720100
O       0    0.53112300   1.04132500   0.61654500
O       0   -2.63391700   0.98544300   0.73823700
O       0   -2.89992100  -1.99388900   0.41277100
O       0   -4.79934100   0.21412500  -1.19728000
In     -1   -3.86392700   4.73405000  -1.08681300
In     -1   -2.69748000  -0.76034800   2.10624400
In     -1   -0.98159100  -2.92023200   0.12248400
In     -1   -4.90725300   1.41236700   0.70754400
In     -1   -4.31717700  -3.66267900   0.06618600
In     -1   -6.60868500  -0.79038700  -1.24362400
In     -1    2.30158000   2.31367000   0.19702000
In     -1    1.17694100  -0.30580400   2.08328600
In     -1    4.51181600   0.14284200   1.59811100
In     -1    5.63775000   3.05649300   0.25564200
In     -1   -1.11660000   2.27364400   0.23241700
In     -1    2.89167800  -2.75993700  -0.44239800
In     -1    6.68260200  -1.89974300  -0.91895000
O      -1   -5.31870400   3.12109000  -0.56676000
O      -1    0.63419300   3.69163700   0.39392400
O      -1    3.60913000   4.03686900   0.39633000
O      -1   -1.83335900   3.96827900  -1.03427200
O      -1   -0.62884000  -1.47433400   1.78682300
O      -1   -4.76577500  -0.04507300   2.42646500
O      -1   -2.32714700  -4.63234900  -0.37864100
O      -1   -6.89892100   0.40812400   0.59228500
O      -1   -5.98527500  -2.28678000   0.26088500
O      -1    2.94266500  -1.37117500   1.22474800
O      -1    6.29190200  -1.04422600   1.03807500
O      -1    2.73141400   1.32989000   2.15757400
O      -1    5.96579800  -0.20329400  -2.18535600
O      -1    5.06091900  -3.28631000  -0.52014300
O      -1    4.29229000   1.34320800  -0.24272900
O      -1    0.89994300  -3.76529900  -0.55879900
C       0   -0.34430400  -0.26536300  -1.62533000
O       0   -1.03472400  -1.37469700  -1.59643900
O       0   -1.05804700   0.80181800  -1.67820800
H       0    0.92428600  -0.25195200  -2.47014600

1-3 0
def2SVP
****
4-7 37-40 0
6-31++G(d,p)
****
8-20 0
LanL2DZ
****
21-36 0
3-21+G
****

1-3 0
def2SVP
8-20 0
LanL2DZ

```

References

- 1 S. Brunauer, P. H. Emmett and E. Teller, *J. Am. Chem. Soc.*, 1938, **60**, 309.
- 2 B. Ravel and M. Newville, *J. Synchrotron Rad.*, 2005, **12**, 537; M. Newville and *J. Synchrotron Rad.*, 2001, **8**, 96.
- 3 S. I. Zabinsky, J. J. Rehr, A. Ankudinov, R. C. Albers and M. J. Eller, *Phys. Rev. B*, 1995, **52**, 2995- 3009.
- 4 J. P. Perdew, K. Burke and M. Ernzerhof, *Phys. Rev. Lett.*, 1996, **77**, 3865; J. P. Perdew, K. Burke and M. Ernzerhof, *Phys. Rev. Lett.*, 1997, **78**, 1396; B. I. Dunlap, *J. Chem. Phys.*, 1983, **78**, 3140.
- 5 R. Gulde, P. Pollak and F. Weigend, *J. Chem. Theory Comput.*, 2012, **8**, 4062; R. Ditchfield, W. J. Hehre and J. A. Pople, *J. Chem. Phys.* 1971, **54**, 724; P. J. Hay and W. R. Wadt, *J. Chem. Phys.*, 1985, **82**, 270; W. R. Wadt and, P. J. Hay, *J. Chem. Phys.*, 1985, **82**, 284; P. J. Hay and W. R. Wadt, *J. Chem. Phys.*, 1985, **82**, 299.
- 6 S. Grimme, J. Antony, S. Ehrlich and H. Krieg, *J. Chem. Phys.* 2010, **132**, 154104.
- 7 J. Perdew, M. Ernzerhof and K. Burke, *J. Chem. Phys.*, 1996, **105**, 9982; C. Adamo and V. Barone, *J. Chem. Phys.*, 1999, **110**, 6158.
- 8 R. Lang, T. Li, D. Matsumura, S. Miao, Y. Ren, Y. T. Cui, Y. Tan, B. Qiao, L. Li, A. Wang, X. Wang and T. Zhang, *Angew. Chem. Int. Ed.*, 2016, **55**, 16054.
- 9 A. V. Marenich, S. V. Jerome, C. J. Cramer and D. G. Truhlar, *J. Chem. Theory Comput.*, 2012, **8**, 527.
- 10 X. Zhang, G. Liu, K. H. M. Broer, G. Ganteför and K. Bowen, *Angew. Chem. Int. Ed.*, 2016, **55**, 9644.